A Lumped Parameter Model of Plasma Focus

José H. González, Alejandro Clausse, Horacio Bruzzone, and Pablo C. Florido

***Abstract*—In this paper, a fast running computer model of a plasma focus device is presented. The model is based on the snowplow model constructed with effective parameters validated against experimental results. A pinch model is included to calculate the temporal evolution of the focal variables. The resulting neutron yield predictions are compared against available data at different pressures, electrode length, and capacitor voltages from experimental measurements, finding good agreements. The model ultimately calculates the neutron production given the geometric parameters and the filling deuterium pressure.**

***Index Terms*—Modeling, neutron sources, plasma focus, plasma pinch, thermonuclear.**

I. Introduction

PLASMA focus is a phenomenon occurring at the open end of coaxial electrodes when an intense electrical discharge between them is induced by external means [1].

Fig. 1 shows a scheme of the system. Two coaxial electrodes are located inside a vacuum chamber filled with deuterium gas at low pressure (neutrons were reported from 0.1 to 10 mbar). A charged capacitor bank is connected to the closed end of the electrodes through a switch (spark-gap). After closing the switch, a gas discharge starts in the gap between the electrodes forming an umbrella-like plasma layer. The azimuthal magnetic field located in the toroidal volume enclosed by the current produces a $\vec{J} \times \vec{B}$ force that pushes the sheath toward the open end of the electrodes. The run-down of the current sheet is a sweeping supersonic shock that propagates collecting, with certain efficiency ξ, the gas particles ahead of the front (snowplow scenario). On its arrival at the open end (some microseconds after triggering), the magnetic field starts to contract, accelerating the plasma toward the axis (run-over stage). Finally, the sheath clashes on the axis in the form of a small dense plasma cylinder (pinch).

Plasma focus (PF) devices have not been commercially developed as neutron sources, being currently restricted to low-cost laboratory equipment for the study of dense plasmas [2], [7].

Optimized PF geometric and operation parameters need to be systematically studied, in order to optimize costs, neutron production, and fluxes [3]. At present, there is no available tool for neutron production design validated with experimental data, sufficiently accurate and fast in order to be used in a multiparameter optimization approach [4].

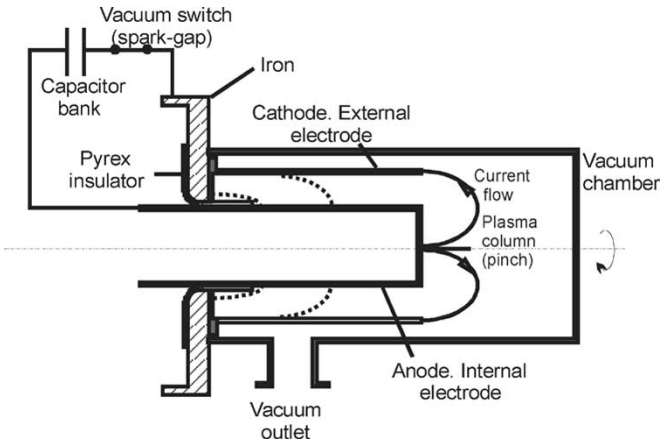

Fig. 1. Scheme of a plasma focus device.

In this work, a fast running computer model is developed in order to predict the neutron production of PF, specially focused in parameters optimization. The kinematics of the current sheet is represented following Lee's model [19]. The model is based on a plane, "two-dimensional" (2-D) snowplow [5], [6] model complemented with sensible estimations for the plasma parameters [8] (density n and temperature T). Using the derived set of differential equations with the snowplow approximation for the breakdown and collapse of the current sheet, and a model for the pinch compression, the neutron production by thermofusion can be estimated if thermal equilibrium is supposed in the plasma. These equations are coupled with the electrical circuit. A powerful numerical integrator for first order differential equations [9] is used, and the code can perform an estimation of the neutron production very quickly.

II. Description of the Model

The evolution of the current sheet is represented by means of planar (axial and radial) shock waves, as it is shown in Fig. 2. Inside the current sheet, homogeneous ionized ideal gas is assumed. The whole process is accordingly divided into three stages: run-down, run-over, and pinch compression.

A. Run-Down

In the run-down, the current sheet is represented by an annular piston moving forward in the axial direction (Fig. 3). The mass and momentum equations of the plasma piston are

$$\frac{dM_X}{dt} = \xi_X \rho_0 \pi \left(R_e^2 - R_i^2\right) V_X \tag{1}$$

$$\frac{d\left(M_X V_X\right)}{dt} = \frac{1}{2} l I^2 \tag{2}$$

Manuscript received October 27, 2003; revised January 2, 2004. This work was supported by the National Atomic Energy Commission and the Laboratorio de Plasmas Densos Magnetizados (PLADEMA), Argentina.

J. H. González and P. C. Florido are with the Centro Atómico Bariloche and Instituto Balseiro, 8400 Bariloche, Argentina (e-mail: pampa@cab.cnea.gov.ar).

A. Clausse is with the National Atomic Energy Commission, CONICET and Universidad Nacional del Centro, 7000 Tandil, Argentina (e-mail: clausse@exa.unicen.edu.ar).

H. Bruzzone is with the CONICET and Universidad Nacional de Mar del Plata, 7600 Mar del Plata, Argentina (e-mail: bruzzone@mdp.edu.ar).

Digital Object Identifier 10.1109/TPS.2004.827573

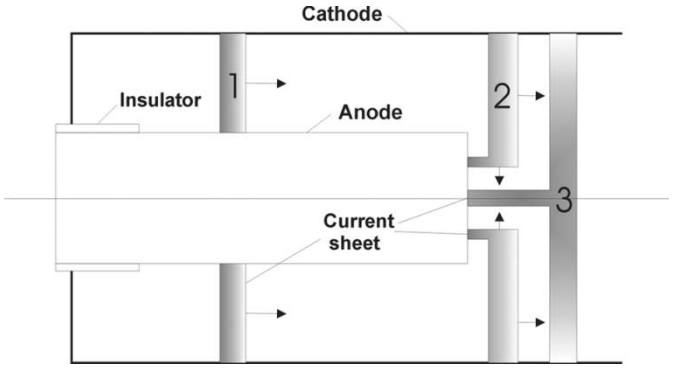

Fig. 2. Planar-sheet model of plasma focus. 1. Run-down. 2. Run-over. 3. Pinch.

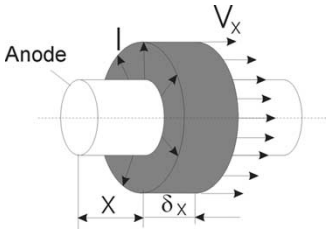

Fig. 3. Run-down stage.

where an axial sweep efficiency ξ_X is introduced to account for shape effects, V_X is the axial piston velocity, ρ_o is the density of the stagnant gas ahead of the piston, R_e and R_i are the cathode and anode radii, and l is the linear inductance of the gun [10]

$$l = \frac{\mu_0}{2\pi} \ln\left(\frac{R_e}{R_i}\right). \tag{3}$$

Assuming that the electric current flows at the backside of the sheet [11], the circuit equation is

$$\frac{d}{dt}\left\{[L_e + lX]\frac{dQ}{dt}\right\} + \frac{Q}{C} = 0 \tag{4}$$

where X is the position of the piston backside, L_e is the inductance of the external circuit, Q is the capacitor charge, and C is the capacity.

B. Run-Over

On the sheet's arrival at the anode open end, the magnetic field accelerates the plasma toward the axis. The radial contraction is modeled by a planar cylinder whose length is determined by the axial piston (Fig. 4). The mass and momentum balances of the radial contraction are

$$\frac{dM_R}{dt} = \xi_R \rho_0 2\pi (R - \delta_R)(X + \delta_X - Z_{\rm INT}) V_R \tag{5}$$

$$\frac{d(M_R V_R)}{dt} = -\frac{\mu_0 I^2}{4\pi}\frac{X - Z_{\rm INT}}{R}. \tag{6}$$

Note that the logarithmic factor, (3), does not appear in (6), since the magnetic pressure is constant over the radial piston area.

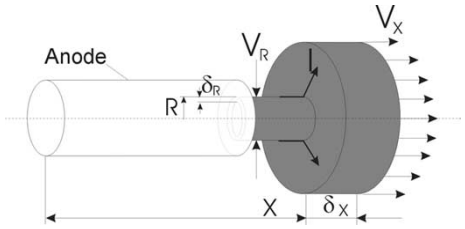

Fig. 4. Run-over stage.

The mass and momentum balance of the axial piston are given by

$$\frac{dM_X}{dt} = \xi_X \rho_0 \pi \left(R_e^2 - R^2\right) V_X \tag{7}$$

$$\frac{d(M_X V_X)}{dt} = \frac{\mu_0 I^2}{4\pi} \ln\left(\frac{R_e}{R}\right). \tag{8}$$

The circuit equation during the run-over stage is

$$\frac{d}{dt}\left[L_{\rm TOT}\frac{dQ}{dt}\right] + \frac{Q}{C} = 0 \tag{9}$$

where $L_{\rm TOT}$ is the total inductance

$$L_{\rm TOT} = L_c + lZ_{\rm INT} + \frac{\mu_0}{2\pi}(X - Z_{\rm INT}) \ln\left(\frac{R_e}{R}\right). \tag{10}$$

Sheet Thickness: The thickness of the axial piston (in both previous stages), δ_X, can be calculated regarding that the mass fraction trapped in the axial portion of the sheet is

$$M_X = \rho_L \upsilon_X = \rho_L \pi \left(R_e^2 - R^2\right) \delta_X. \tag{11}$$

In (11), the sheet density is considered proportional to ρ_0 (i.e., $\rho_L = K\rho_0$, K being the snowplow compression factor), and $R = R_i$ in the run-down stage.

Similarly, the radial thickness during the radial stage can be calculated from the mass fraction trapped in the radial portion of the sheet

$$M_R = \rho_L \upsilon_R = \rho_L \pi \left[R^2 - (R - \delta_R)^2\right](X + \delta_X - Z_{\rm INT}). \tag{12}$$

Energy balance: From the global energy balance of the system (taking into account kinetic, electromagnetic and internal energies), it can be shown that the rate of internal energy gain in the pistons is given by [20]

$$\frac{dE_R^{\rm INT}}{dt} = \frac{V_R^2}{2}\frac{dM_R}{dt} \tag{13}$$

$$\frac{dE_X^{\rm INT}}{dt} = \frac{V_X^2}{2}\frac{dM_X}{dt} \tag{14}$$

it should be stressed that V_R and V_X are time dependent.

Also relevant in the pinch compression are the magnetic energy and the electric energy remaining in the capacitors

$$E_{\rm MAG} = \frac{1}{2} L_{\rm TOT} I^2 \tag{15}$$

$$E_{\rm CAP} = \frac{1}{2}\frac{Q^2}{C}. \tag{16}$$

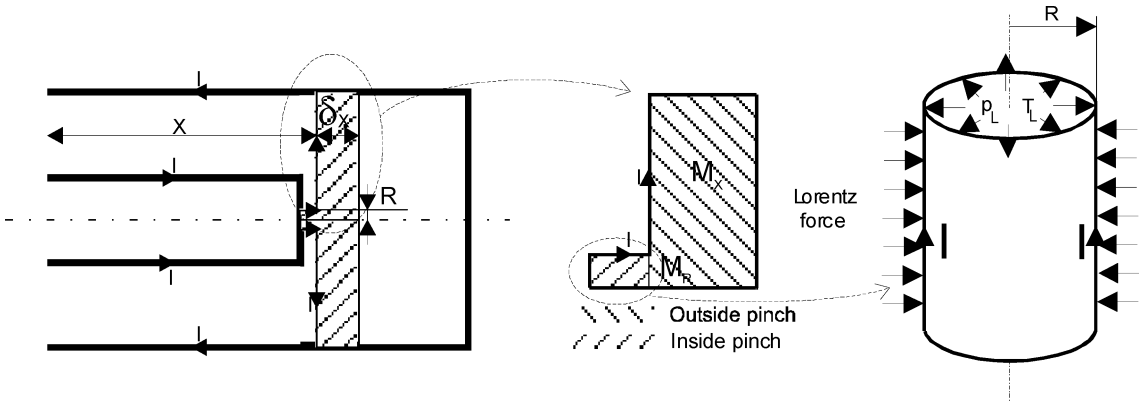

Fig. 5. Diagram of the pinch model.

C. Pinch Compression

The pinch compression starts when the front of the radial piston reaches the axis (i.e., $R - \delta_R = 0$). In order to calculate the temporal evolution of the pinch volume (Fig. 5), the momentum balance inside the pinch cylinder is written as

$$\frac{\partial(\rho v_r)}{\partial t} + \frac{1}{r}\frac{\partial\left(r\rho v_r^2\right)}{\partial r} = J_X B_\theta - \frac{\partial p}{\partial r} \tag{17}$$

where ρ is the mass density, J_X is the axial current density, B_θ is the azimuthal magnetic field, and p is the pressure.

The pressure is related to the temperature by means of the ideal gas equation [12]. Here, it is assumed that the number of ions is equal to the number of electrons (i.e., $N_e = N_i$) and that there is thermal equilibrium between them (i.e., $T_e = T_i$), which leads to

$$p(x,r,t)v(t) = N_e k T_e + N_i k T_i = N k T(x,r,t) \tag{18}$$

where $v(t)$ is the pinch volume and $N = N_e + N_i$.

Inside the pinch, the gas heats up due to the transformation of kinetic energy into internal energy during the collapse in the axis. The energy balance of the system during the pinch is given by

$$E_{\rm TOT} = E_{\rm CAP} + E_{\rm MAG} + E_X^{\rm INT} + E_X^{\rm KIN} + E_{\rm PINCH}^{\rm INT} + E_{\rm PINCH}^{\rm KIN}. \tag{19}$$

The total energy, $E_{\rm TOT}$, is invariant during the evolution, and equals the initial capacitor energy. The first two terms in (19) are given by (16) and (15). The internal energy of the axial piston, $E_{\rm INT}^X$, is calculated using (14), whereas the corresponding kinetic energy is given by

$$E_X^{\rm KIN} = \frac{1}{2} M_X V_X^2. \tag{20}$$

The kinetic energy contained in a differential volume, dv, located at the point (x,r) inside the pinch is

$$dE_{\rm PINCH}^{\rm KIN} = \frac{1}{2} V^2(x,r,t)\rho dv \tag{21}$$

where ρ is the mass density and $V(x,r,t)$ is the modulus of the velocity field.

The local temperature is proportional to the internal energy per particle, that is

$$T(x,r,t) = \frac{(\gamma-1)}{k}\frac{E_{\rm PINCH}^{\rm INT}(x,r,t)}{N} \tag{22}$$

where $\gamma = 5/3$ for deuterium [12], k is the Boltzmann constant.

In order to calculate the kinetic energy inside the pinch, the velocity distribution should be provided. After the sheet front reaches the axis, a shock wave reflection starts at $r = 0$ proceeding toward the pinch external face $(r = R)$, which in turn is moving toward the axis. The detailed modeling of this phenomenon would involve the solution of the compressible MHD equations. An alternative lumped parameter approach to this problem is to postulate a family of velocity distributions, which satisfy the expected boundary conditions, namely:

a) zero radial velocity at the axis;
b) at the pinch external face $(r = R)$, the radial velocity is the radial velocity of the current sheet, $V(t)$;
c) since there is no external magnetic pressure in the axial direction, the pinch expands in this direction at sound velocity C [13].

Assuming for simplicity a constant power law dependence of the radial component with the radial coordinate satisfying conditions (a) and (b), the expression of the velocity profile results in

$$v_r(x,r,t) = \left(\frac{r}{R(t)}\right)^a V(t)$$
$$v_x(x,r,t) = \frac{x}{h(t)} C(t) \tag{23}$$

where h is the pinch height, C is the average sound velocity at $x = h$, R is the pinch radius, V the velocity of the radial piston, and a is an effective constant parameter.

Replacing (23) in (21) and integrating over the pinch volume, the kinetic energy of the pinch results in

$$E_{\rm PINCH}^{\rm KIN} = \frac{N m_i}{4}\left[\frac{C^2}{3} + \frac{V^2}{a+1}\right]. \tag{24}$$

In (24), the mass of the electrons was neglected, and m_i is the mass of the ions.

Combining (17)–(24) and assuming for simplicity uniform mass density and electrical current concentrated in the external

TABLE I
PARAMETERS OF EXPERIMENT [17]

Symbol	Parameter	Value
C	Capacity	32.7 μF
V	Charge voltage	11 kV
L_e	External inductance	80 nHy
Z_{INT}	Anode length	11 to 21 cm
R_i	Anode radius	0.9 cm
R_e	Cathode radius	5 cm

TABLE II
PARAMETERS OF EXPERIMENT [18]

Symbol	Parameter	Value
C	Capacity	10.5 μF
V	Charge voltage	30 kV
L_e	External inductance	39 nHy
Z_{INT}	Anode length	8.7 cm
R_i	Anode radius	1.9 cm
R_e	Cathode radius	3.6 cm

border, (17) can be integrated over the pinch volume, leading to [14]

$$\frac{d}{dt}(\rho V R^2) = (a+2)R\left[p_{\text{eff}} - p_M\right] \tag{25}$$

where p_M is the magnetic pressure [15]

$$p_M = \frac{\mu_0 I^2}{8\pi R^2} \tag{26}$$

and p_{eff} is an effective counterpressure given by

$$p_{\text{eff}} = \frac{2}{m_i}(\gamma-1)\rho\left\{\frac{E_{\text{PINCH}}^{\text{INT}}}{N} + \frac{E_{\text{PINCH}}^{\text{KIN}}}{N} - \frac{m_i}{2}\left[\frac{2}{3}C^2 + \frac{1}{4a+2}V^2\right]\right\} \tag{27}$$

where $E_{\text{PINCH}}^{\text{INT}}$ is calculated from (19).

Neutron production: The neutron production is calculated assuming a thermonuclear model. Accordingly, it is given by

$$\frac{dY}{dt} = \int_{\mathcal{V}} \frac{1}{2} n^2 \langle \sigma v \rangle d\mathcal{V} \tag{28}$$

where $\mathcal{V}$ is the volume of the pinch column and n is the number density of deuterons, $n = N/\mathcal{V}$. The average fusion cross section $\langle \sigma v \rangle$ depends on the temperature according to [16]

$$\langle \sigma v \rangle = 1.168\, 10^{-18} T^{-2/3} e^{-187.6 T^{-1/3}} \tag{29}$$

where T is expressed in electronvolts, and $\langle \sigma v \rangle$ in m^3/s.

Using (19)–(29), the integral in (28) is numerically calculated by means of the trapezium method.

III. MODEL VALIDATION

The complete system of ordinary differential equations that describe the operation of a plasma focus are (1) and (2), (4)–(9), (13) and (14), (25) and (28). The equations were solved using the FORTRAN LSODE subroutine package [9].

In order to validate the model, the numerical results were compared against experimental measurements of the neutron pulses generated in two Mather-type plasma focus available in the open literature [17], [18]. Tables I and II detail the geometric and electrical parameters of the devices. Systematic measurements of the neutron yield dependence with the deuterium pressure were reported in [17], including a study of the influence of the anode length on the neutron yield and the optimum pressure. In [18] the time to the pinch, the maximum current and the neutron yield as functions of the filling pressures are provided.

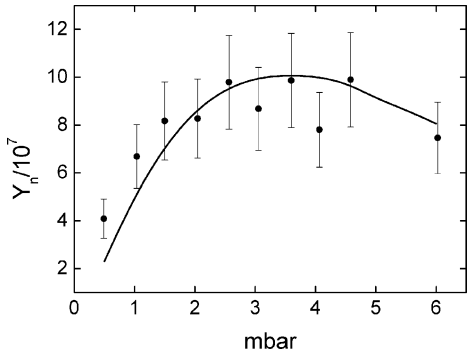

Fig. 6. Neutron emission versus deuterium filling pressure for experiment [17]. Experimental data (points) and numerical calculation (curve).

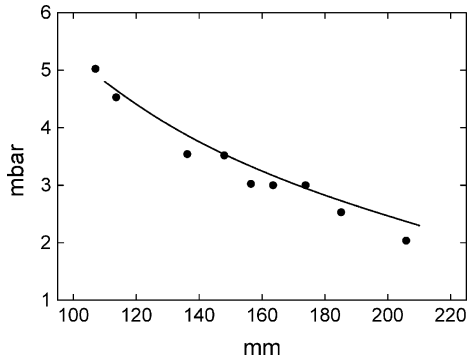

Fig. 7. Optimum filling pressure versus the anode length for experiment [17]. Experimental data (points) and numerical calculation (curve).

Fig. 6 compares the dependence of the neutron yield with the deuterium pressure in discharges over a 14.8-cm anode for [17]. The value of the effective parameters ξ_X, ξ_R, and a (see Table IV) were adjusted to minimize the discrepancies between the experimental data and the numerical results. The compression factor K was set in 4, which is a typical value for planar supersonic shock waves.

Fig. 7 compares the pressure at which the optimum neutron production occurs, for several anode lengths. Although there are no error bars available for these data, there is a very good agreement between calculated and measured values.

Fig. 8 compares the influence of the anode length on the maximum neutron yield at the optimum deuterium pressure. It can be seen that there is a good agreement between the model and the experiments, regarding that the same set of effective parameters was used in all the calculations.

Finally, Fig. 9 shows the dependence of neutron production with anode length and deuterium filling pressure, where the po-

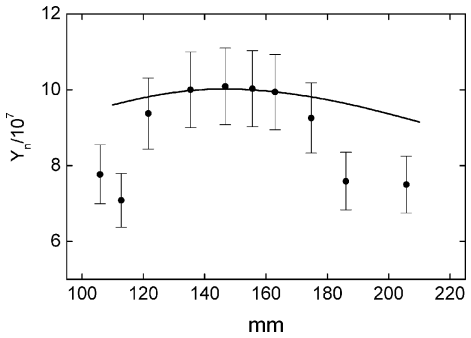

Fig. 8. Maximum neutron emission versus anode length for experiment [17]. Experimental data (points) and numerical calculation (curve).

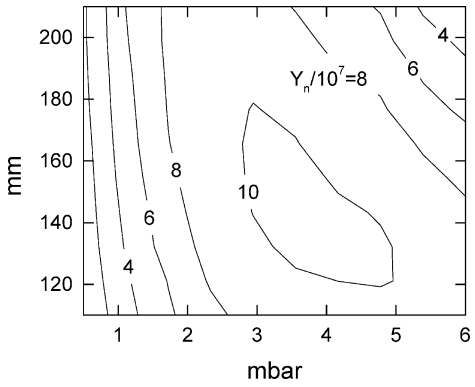

Fig. 9. Contour map of the neutron yield in the parameter plane (p_o, Z) for experiment [17].

TABLE III
MAIN VARIABLES FOR OPTIMUM NEUTRON PRODUCTION IN EXPERIMENT [17]

Symbol	Quantity	Value
Y^{OPT}	Optimum neutron production	1.0 10^8
Z^{OPT}	Z_{INT} for Y^{OPT} [cm]	15
p^{OPT}	p_0 for Y^{OPT}	3.7
I_{MAX}	Maximum electric current [A]	153660
I_{PINCH}	Electric current at pinch compression [A]	152066
t_{PINCH}	Time elapsed to pinch occurrence [μs]	2.27

sition of the optimum neutron production can be observed. The main variables of this maximum are in Table III.

The effective parameters required to numerically reproduce the experiments reported in [18] are shown in Table IV. Fig. 10 compares the measured time to focus in [18] with the calculations of the present model. Figs. 11 and 12 show the corresponding pressure dependence of the maximum current and the neutron yield. The agreement found in Figs. 10 and 11 supports the modeling of the current sheet dynamics, whereas the model performance in describing the neutron production (Fig. 12) suggests that the pinch model is valid over a wide pressure range.

IV. STUDY OF A REFERENCE CASE

In order to study the behavior of the relevant variables during simulation of plasma focus discharges, a reference case based in the experiment [17] was studied (see Table I), using the model

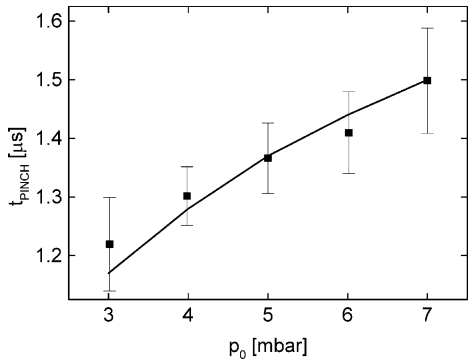

Fig. 10. Pressure dependence of the time to pinch for experiment [18]. Experimental data (points) and numerical calculation (curve).

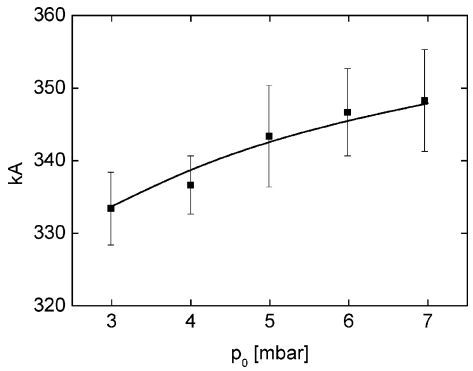

Fig. 11. Pressure dependence of the maximum electric current for experiment [18]. Experimental data (points) and numerical calculation (curve).

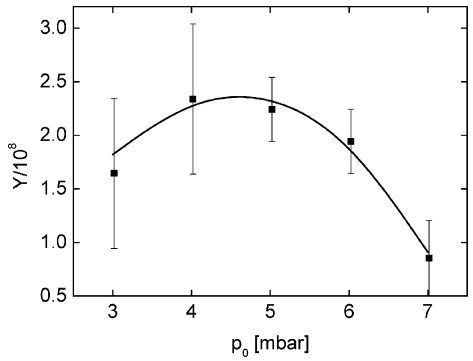

Fig. 12. Pressure dependence of the neutron yield for experiment [18]. Experimental data (points) and numerical calculation (curve).

parameters shown in the third column of Table IV. The reference case assumes the following operating conditions.

Filling pressure: 3.7 mbar.
Anode length: 150 mm.
Charging voltage: 12 kV.

Fig. 13 shows the temporal evolution of the electrical current. Basically, it follows a quarter of period of an LC circuit, shaped by the inductance variation of the coaxial gun [(4) and (9)]. The current drop at 2.27 μs is caused by the inductance jump during the pinch, when the pinch radius, R, reaches the minimum value [see (10)].

Fig. 14 shows the evolution of the total mass of the current sheet (i.e., accumulated in all the pistons). After an initial transient, the accumulation rate remains constant. The velocity of

TABLE IV
EFFECTIVE PARAMETERS

Symbol	Quantity	Experiment [17]	Experiment [18]
ξ_X	Axial sweep efficiency	0.08	0.4
ξ_R	Radial sweep efficiency	0.16	0.015
a	Radial velocity profile exponent	0.07	0.5

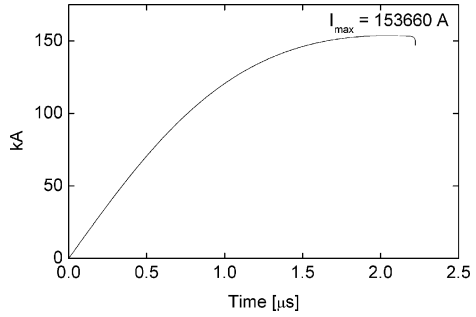

Fig. 13. Temporal evolution of the electrical current.

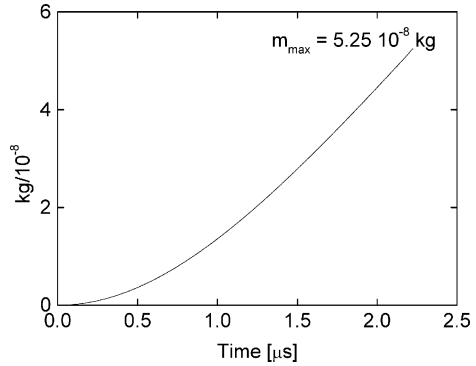

Fig. 14. Evolution of the mass accumulated in all the pistons.

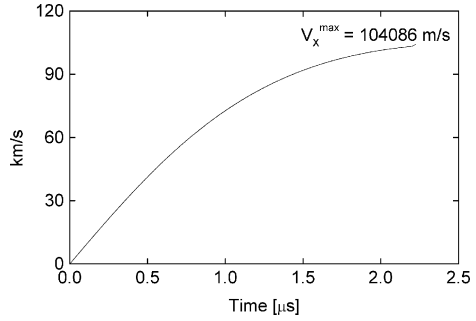

Fig. 15. Velocity of the axial piston during the run-down.

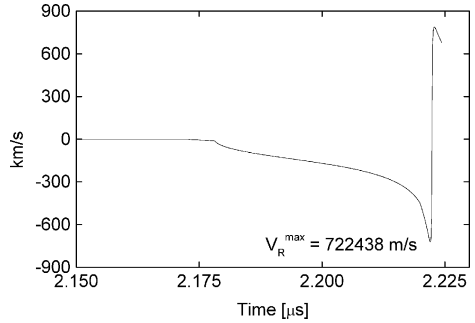

Fig. 16. Velocity of the radial piston.

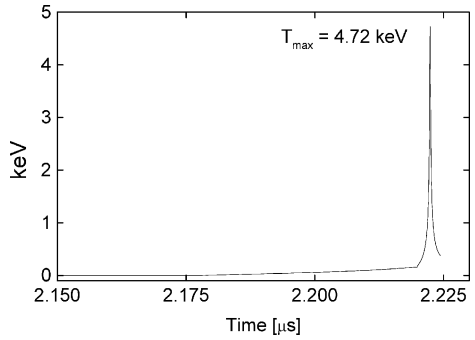

Fig. 17. Average pinch temperature.

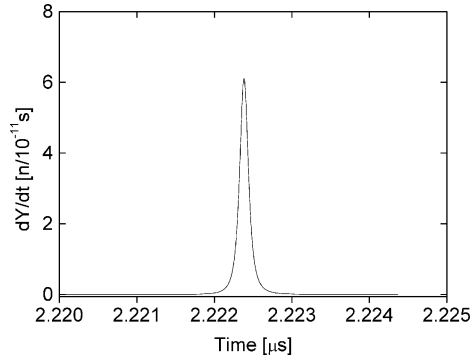

Fig. 18. Evolution of the neutron rate.

the axial piston is shown in Fig. 15. It can be seen that the axial velocity basically accompany the current behavior [(2)].

Fig. 16 shows the velocity of the radial piston. At 2.172 μs, the axial piston begins to run over the anode. Then the radial piston is strongly accelerated toward the axis. At 2.2 μs, the radial front touches the axis, and the pinch begins. The minimum radius is reached at 2.2225 μs.

Fig. 17 shows the temperature evolution of the radial piston. There is a slight increase during the radial collapse, followed by the temperature excursion during the pinch compression. The maximum predicted temperature is 4.8 keV, whereas the time-average pinch temperature is 887.94 eV. Finally, Fig. 18 shows the evolution of the neutron rate. The total neutron production calculated by the model agrees with the experimental data. However, the calculated duration of the pinch (5 ns) is much shorter than what was measured in other experiments (about 100 ns). This effect requires further investigation.

V. SENSIBILITY ANALYSIS

Since the numerical results depends on the value of three effective parameters (ξ_X, ξ_R, a) that should be estimated by com-

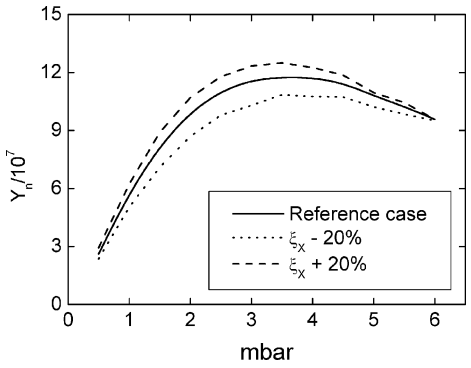

Fig. 19. Sensibility of the neutron emission curve to the parameter ξ_X.

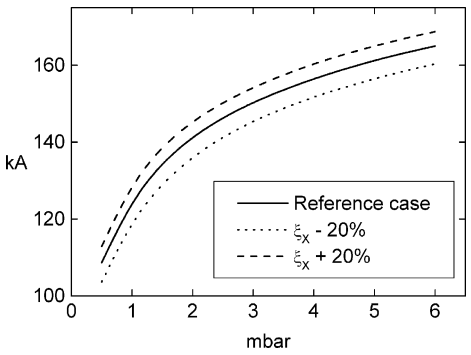

Fig. 20. Sensibility of the maximum electrical current to the parameter ξ_X.

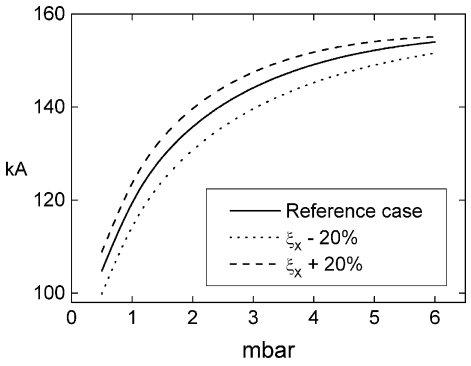

Fig. 21. Sensibility of the pinch current to the parameter ξ_X.

parison against experimental data, it is important to study the sensibility of the model to variations of these parameters. First, the impact of the effective parameters on the dependence of the main observable variables with the filling pressure was analyzed. Figs. 19–22 show the sensibility of the neutron production, the maximum current, the pinch current, and the time to the focus, to variations of ξ_X. Reducing ξ_X, the neutron yield decreases and the optimum pressure increases. Similarly, the currents and the pinch time increases with ξ_X.

On the other hand, changes in ξ_R and a only affects substantially the neutron yield. Figs. 23 and 24 show the sensibility of Y to ξ_R and a. Reducing ξ_R, the neutron yield and the optimum pressure decrease. Increasing a reduces the neutron yield, but does not affect the optimum pressure.

Figs. 25–27 show the effect of the effective parameters on the optimum plasma-focus design (i.e., the value of the main

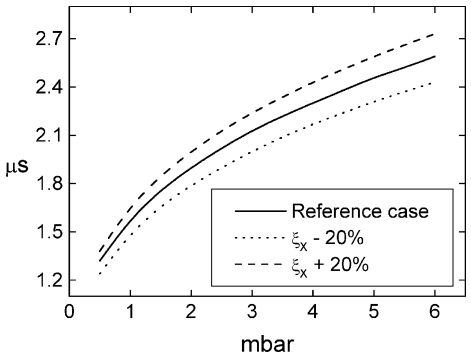

Fig. 22. Sensibility of the pinch time to the parameter ξ_X.

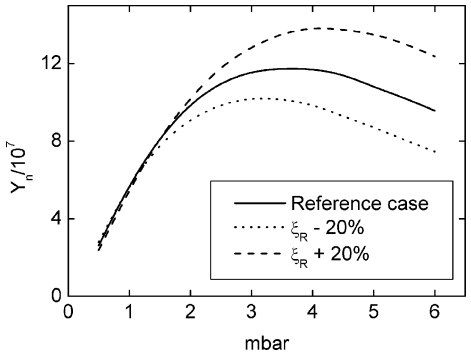

Fig. 23. Sensibility of the neutron yield curve to the parameter ξ_R.

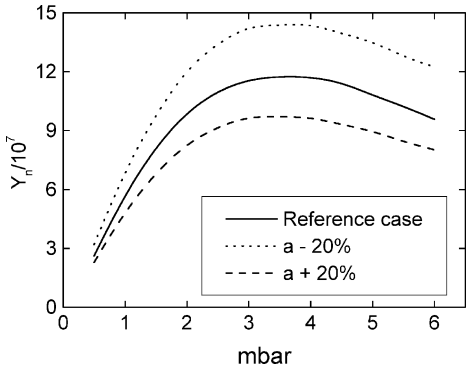

Fig. 24. Sensibility of the neutron emission curve to the pinch parameter a.

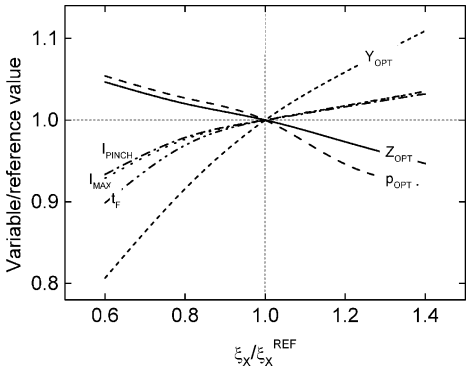

Fig. 25. Sensibility analysis to variations of the parameter ξ_X.

variables in the maximum of Fig. 9). The largest impact was observed in the sensibility of the optimum neutron production and the optimum pressure to variations of ξ_R.

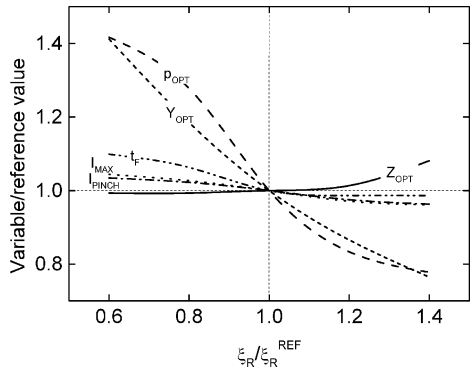

Fig. 26. Sensibility analysis to variations of the parameter ξ_R.

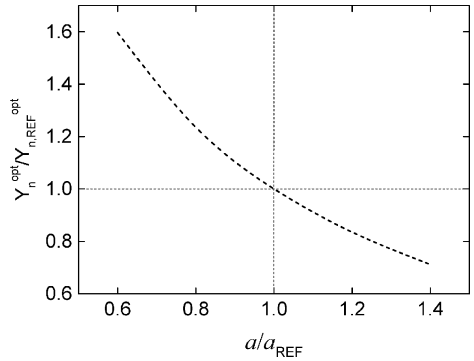

Fig. 27. Sensibility of the optimum neutron yield to the pinch parameter a.

VI. Conclusion

A lumped parameter model for the operation and neutron production of plasma-focus devices was presented. The resulting neutron yield predictions have been tested with available data at different pressures and cathode length. The model explains very well the dependence of the experimental data with the filling pressure and anode length in two different devices.

The results show that the hypothesis of thermonuclear reactions as the main source of the neutrons seems to be sufficient for obtaining most of the measured features of the neutron yield.

It is true that there is a significant literature, especially from Europe, that clearly shows the existence of beam-driven fusion reactions in the plasma focus. However, it is also clear that the devices in this paper are being operated in the high pressure regime. Thus, a better comparison is with the Mather group literature from Los Alamos. That group clearly showed a scaling dependence of the fusion yield proportional to the current to the fourth.

A possible interpretation of what happened with the beams inside the focus can be obtained by observing that the ion–electron and ion–ion equilibrium times go as $1/I$. Therefore, as the current increases, beam contributions to the fusion yield via beam-hot target interactions become heating contributions to the core pinch.

The sensibility study showed that the effective kinetic parameters ξ_X and ξ_R impact on the neutron production as well as the pressure dependence. Decreasing ξ_X shifts the optimum pressure to higher values, whereas the opposite occurs with ξ_R. Higher values of ξ_X and lower values of ξ_R increase the sensibility of the neutron yield to pressure variations. The parameter a (effective velocity profile) modifies only the level of neutron emission.

In order to identify proper correlations of the parameters with geometries and electrical parameters, more experimental data should be confronted. Some efforts were recently directed toward that end, with the comprehensive characterization of new small plasma focus devices [21]–[24]. For future experiments, we suggest systematic measurements of the pressure dependence of neutron yield, maximum and pinch currents, and time to focus. In addition, it would be useful to characterize as accurate as possible the electrical parameters, such as inductances, resistances, and spark gap response curves.

The numerical pinch duration was about 5 ns, which is much shorter than the corresponding experimental measurements (about 50–100 ns). A possible explanation of this discrepancy is that the present model calculates the pinch as a single rigid cylinder, whereas actual observations suggest the occurrence of a train of micropinches caused by $m = 0$ instabilities.

The dependence of the optimum neutron yield with the anode length was fairly reproduced by the numerical results (Fig. 8). However, some discrepancy persisted that could not be overcome by tuning the effective parameters. Probably this is caused by the impossibility to model correctly the mass expulsion through the cathode bars. The extension of the model to account for the latter and other effects not included in the present description would be an interesting issue for further investigations.

The supporting evidence presented in this paper does not preclude interpretation by other models, but the model set out here does at least facilitate the raising of hypothesis, and offers a simple and complete model for the evaluation and design of the dynamics and neutron production of plasma focus devices.

Acknowledgment

The authors wish to thank two anonymous reviewers for their comments and observations that helped to enhance the quality of this paper.

References

[1] A. Bernard, P. Cloth, H. Conrads, A. Coudeville, G. Gourlan, A. Jobs, Ch. Maisonnier, and J. P. Rager, "The dense plasma focus—A high intensity neutron source," *Nucl. Instrum. Methods*, vol. 145, pp. 191–218, 1977.

[2] K. H. Kwek, T. Y. Tou, and S. Lee, "Current sheath structures of the plasma focus in the run down phase," *IEEE Trans. Plasma Sci.*, vol. 18, pp. 826–830, Oct. 1990.

[3] P. G. Eltgroth, "Comparison of plasma focus calculations," *Phys. Fluids*, vol. 25, pp. 2408–14, 1982.

[4] C. Moreno, H. Bruzzone, J. Martínez, and A. Clausse, "Conceptual engineering of plasma focus thermonuclear pulsors," *IEEE Trans. Plasma Sci.*, vol. 28, pp. 1735–1741, Oct. 2000.

[5] A. Shock, "Electromagnetic acceleration of plasma for space propulsion," *Planet. Space Sci.*, vol. 4, pp. 133–144, Jan. 1961.

[6] N. F. Tsagas, G. L. R. Moir, and A. E. Prinn, "Retrograde ionizing waves in the coaxial accelerator," *Phys. Lett. A*, vol. 58, pp. 315–317, Sept. 1976.

[7] Q. Niansheng, S. F. Fulhum, R. R. Prasad, and M. Krishnan, "Space and time resolved electron density and current measurements in a dense plasma focus Z-pinch," *IEEE Trans. Plasma Sci.*, vol. 26, pp. 1127–1137, Aug. 1998.

[8] J. H. González, A. Clausse, and P. C. Florido, "An engineering approach for plasma neutron pulsors," in *Proc. 2001: A Nuclear Odyssey*, College Station, TX, 2001.

[9] A. C. Hindmarsh *et al.*, "Odepack, a sistematized collection of ODE solvers," in *Scientific Committing*, R. S. Stepleman *et al.*, Eds. Amsterdam, The Netherlands: North Holland, 1983, p. SS-64.
[10] S. Frish and A. Timoreva, *General Physics Course (Book Style)*. Moscow, U.S.S.R.: Mir, 1973, vol. II, p. 481.
[11] G. Harnwell, *Principles of Electricity and Magnetism (Book Style)*, 2nd ed. New York: McGraw-Hill, 1949, p. 585.
[12] F. F. Huang, *Engineering Thermodynamics—Fundamentals and Applications (Book Style)*. New York: MacMillan, 1994, p. 165.
[13] A. H. Shapiro, *The Dynamics and Thermodynamics of Compressible Fluid Flow (Book Style)*. New York: Ronald, 1953, vol. I, p. 112.
[14] M. R. Spiegel, *Mathematical Handbook (Book Style)*. New York: McGraw-Hill, 1978, p. 95.
[15] N. A. Krall and A. W. Trivelpiece, *Principles of Plasma Physics (Book Style)*. New York: McGraw-Hill, 1973, p. 123.
[16] J. D. Huba, *NRL Plasma Formulary, Beam Physics Branch, Plasma Physics Division*. Washington, DC: Naval Research Lab., 1998, p. 45.
[17] F. N. Beg, M. Zakaullah, M. Nisar, and G. Murtaza, "Role of the anode length in a Mather-type plasma focus," *Mod. Phys. Lett. B*, vol. 6, pp. 593–597, 1992.
[18] C. Moreno, A. Clausse, J. Martínez, J. H. Gonzalez, H. Bruzzone, R. Llovera, A. Tartaglione, and S. Jaroszewicz, "Operation and output characteristics of a small-chamber plasma focus," in *Regional Meeting on Plasma Research in 21st Century*, Bangkok, Thailand, May 2000.
[19] S. Lee, "A new theory for the fast compressional pinch," in *Proc. 1983 College on Plasma Physics*, vol. 2, Trieste, Italy, pp. 967–977.
[20] J. Cole, "Newtonian flow theory for slender bodies," *J. Aeronaut. Sci.*, vol. 24, p. 448, 1957.
[21] L. Soto, A. Esaulov, J. Moreno, P. Silva, G. Sylvester, M. Zambra, A. Nazarenko, and A. Clausse, "Transient electrical discharge in small devices," *Phys. Plasma*, vol. 8, p. 2572, 2001.
[22] P. Silva, L. Soto, J. Moreno, G. Sylvester, M. Zambra, L. Altamirano, H. Bruzzone, A. Clausse, and C. Moreno, "A plasma focus driven by a capacitor bank of tens of Joules," *Rev. Sci. Instrum.*, vol. 73, p. 2583, 2002.
[23] J. Moreno, P. Silva, and L. Soto, "Optical observations of the plasma motion in a fast plasma focus operating at 50 Joules," *Plasma Sources Sci. Technol.*, vol. 12, p. 39, 2003.
[24] P. Silva, J. Moreno, L. Soto, L. Birstein, R. Mayer, and W. Kies, "Neutron emission from a fast plasma focus of 400 Joules," *Appl. Phys. Lett.*, vol. 83, p. 3269, 2003.

José H. González received the nuclear engineering degree from Instituto Balseiro, Bariloche, Argentina, in 1994. Currently, he is with the National Atomic Energy Commission of Argentina and is working toward the Ph.D. degree in nuclear engineering at the Instituto Balseiro.

He is an Instructor of Nuclear Engineering at the University of Cuyo, Argentina.

Alejandro Clausse received the nuclear engineering degree and Ph.D. degree from Instituto Balseiro, Bariloche, Argentina, in 1981 and 1986, respectively.

He is Professor of Engineering at Universidad Nacional del Centro, Argentina. He was a visiting scholar to the Rensselaer Polytechnic Institute, New York, from 1987 to 1990. Currently, he heads the PLADEMA Center of the Interinstitutional Program of Dense Plasmas, and the advanced reactors program of the National Atomic Energy Commission, Argentina.

Dr. Clausse is a Fellow of the National Science and Technology Council of Argentina (CONICET).

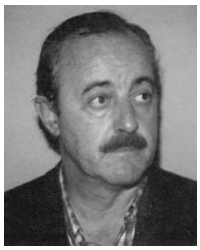

Horacio Bruzzone received the M.Sc. and Ph.D. degrees in physics from the University of Buenos Aires, Buenos Aires, Argentina, in 1967 and 1976, respectively.

From 1981 to 1998, he was Associate Professor of Physics at the University of Buenos Aires and headed the experimental plasma physics group at the Institute of Plasma Physics, Buenos Aires. Since 1999, he had been head of the Fast Pulsed Discharges Laboratory, University of Mar del Plata, Argentina. He is currently chairman of the scientific committee for the International Centre on Dense Magnetized Plasmas (Poland). His research interests are plasmas produced using fast pulsed discharges, with emphasis in plasma focus and Z-pinch devices.

Dr. Bruzzone is a Fellow of the National Science and Technology Council of Argentina (CONICET).

Pablo C. Florido received the nuclear engineering degree and Ph.D. degree from Instituto Balseiro, Bariloche, Argentina, in 1988 and 2002, respectively.

He is Assistant Professor of Nuclear Engineering, University of Cuyo, Argentina. Currently, he heads the division of innovative nuclear design and economic evaluation, the advanced uranium enrichment project of the National Atomic Energy Commission of Argentina, and is safeguards inspector of IAEA.